AJNR Am J Neuroradiol 26:313–318, February 2005

Technical Note

Visualization of Aneurysmal Contours and Perianeurysmal Environment with Conventional and Transparent 3D MR Cisternography

Toru Satoh, Megumi Omi, Chika Ohsako, Atsushi Katsumata, Yusuke Yoshimoto, Shoji Tsuchimoto, Keisuke Onoda, Koji Tokunaga, Kenji Sugiu, and Isao Date

Summary: We have developed conventional and transparent 3D MR cisternography to investigate the spatial relationship between the contours of aneurysmal complex and the perianeurysmal structures including the cranial nerves, dural fold, cranial base bone, and brain parenchyma. Volume data obtained by a T2-weighted 3D fast spin-echo sequence were reconstructed by using a perspective volume-rendering algorithm with a transluminal imaging technique. 3D MR cisternograms provide useful anatomic information in the therapeutic and follow-up management of unruptured cerebral aneurysms.

MR cisternograms obtained by using a T2-weighted 3D fast spin-echo sequence can delineate the outer-wall configuration of the cisternal structures with thin sections and a high signal-to-noise ratio. In the present study, the spatial relationship of the aneurysmal contours to adjacent structures was investigated by using conventional and transparent 3D MR cisternography. Perspective views of the aneurysmal complex depicted by the 3D MR cisternography were correlated with findings disclosed by 3D MR angiography and 3D CT angiography as well as intraoperative anatomic findings acquired by similar visual projections.

Technique

MR Cisternographic Data Acquisition

Two patients with unruptured internal carotid–posterior communicating artery aneurysms that were incidentally detected at MR angiography underwent MR cisternography before prophylactic aneurysmal microneurosurgery. MR cisternography was performed with a clinical MR imager (Signa HiSpeed 1.0T; General Electric Medical Systems, Milwaukee, WI) by using a T2-weighted 3D fast spin-echo sequence. The following parameters were used: 4000/140/1 (TR/ TE/NEX); echo train length, 64; bandwidth, 15.63 KHz; matrix, 256 × 256; section thickness, 1.2 mm; section interval,1.2 mm; field of view, 16 cm; and total imaging time, 8 minutes 1 second. A total of 26 continuous source axial images were acquired. Volume data were transferred to an independent workstation with medical visualization software (Zio M900 Quadra; AMIN, Tokyo, Japan).

Reconstruction of Conventional 3D MR Cisternograms

Data were interpolated every 0.6 mm on a workstation and then processed into the 3D volume-rendering data set (51 data points) in 9 seconds. The conventional 3D MR cisternograms were rendered from the data set in 11 seconds by using a perspective volume-rendering algorithm (1, 2). The signal intensity histogram (arbitrary unit distribution) drawn on the source axial image of the MR cisternogram, the parent internal carotid artery, an aneurysm, the anterior clinoid process bone, and the petroclinoidal dural fold showed profoundly low signal intensity (50–100); juxtacisternal brain and optic nerve, moderately low signal intensity (250–300); and surrounding CSF, profoundly high signal intensity (500–750).

To visualize the margin of the vessels, nerves, and brain parenchyma in three dimensions, the entire area that was hypointense relative to CSF was selected from the opacity chart of the signal intensity distribution by using a function of a square curve with a threshold range of 100–500 (100% opacity level) color-rendered in green (threshold range 100–490) and red (490–500), respectively (Fig 1A). The conventional 3D cisternograms depicted the contours of intracisternal objects (i.e., cranial nerves, vessels, an aneurysm) and juxtacisternal structures (i.e., cranial base bone, dura mater, ligament, and the brain); those images were observed from various intracisternal viewpoints with a visual angle of 90°.

Reconstruction of Transparent 3D MR Cisternograms

The transparent 3D MR cisternograms were rendered from the same data set by using a perspective volume-rendering algorithm with transluminal imaging technique (2–4). Transparency of the borderline between the cisternal and juxtacisternal structures was selected from the same opacity chart by using a function of a square curve with a threshold range of 480–500 (100% opacity level) color-rendered in green (threshold range 480–490) and red (490–500), respectively (Fig 1B). To visualize the profoundly hypointense arterial component, another square curve with a threshold range of 100–250 (100% opacity level) was employed and color-rendered in blue. Those transparent images represented the contours of the cisternal structures, including an aneurysmal complex and juxtacisternal brain as a series of rings, so the underlying objects were directly depicted through the spaces between the rings.

Received July 4, 2004; accepted after revision August 24.

Presented in part at the 62nd Annual Meeting of the Japan Neurosurgical Society, October 1, 2003, Sendai, Japan.

From the Departments of Neurological Surgery (T.S.) and Diagnostic Radiology (M.O., C.O.), Ryofukai Satoh Neurosurgical Hospital, Hiroshima, Japan; Department of Neurological Surgery (A.K., Y.Y., S.T.), Onomichi Municipal Hospital, Hiroshima, Japan; and Department of Neurological Surgery (K.O., K.T., K.S., I.D.), Okayama University Graduate School of Medicine and Dentistry, Okayama, Japan.

Address correspondence and reprint requests to Toru Satoh, MD, Department of Neurological Surgery, Ryofukai Satoh Neurosurgical Hospital, 5-23-23 Matsunaga, Fukuyama, Hiroshima, 729-0104.

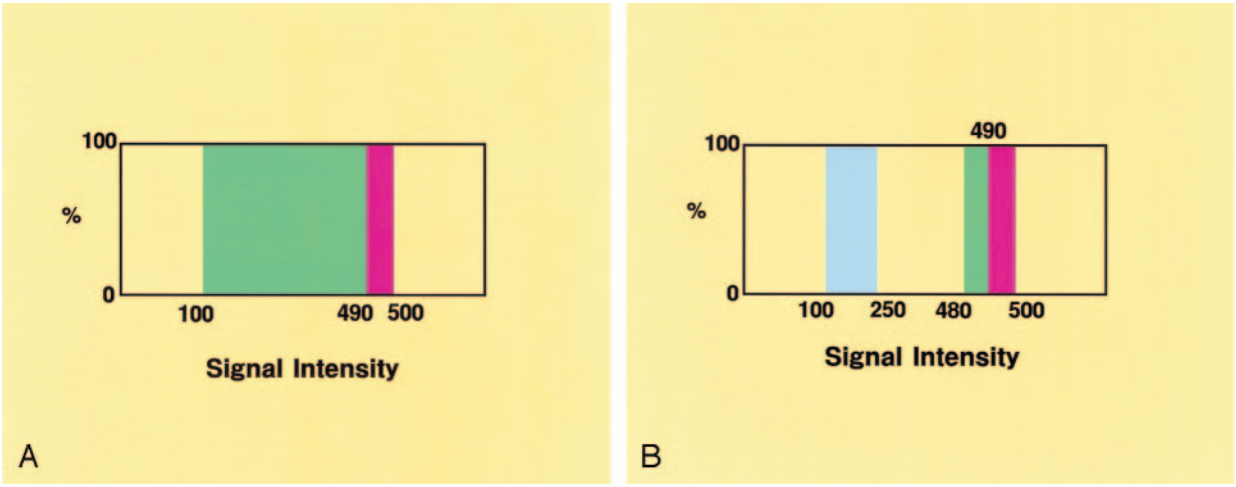

FIG 1. Opacity charts of the signal intensity distribution for the 3D MR cisternograms.

A, Opacity chart for the conventional 3D MR cisternogram, showing a square curve with a threshold range of 100–500 (100% opacity level), and color-rendered in green (threshold range 100–490) and red (490–500).

B, Opacity chart for the transparent 3D MR cisternogram, showing square curves, one with a threshold range of 480–500 (100% opacity level), color-rendered in green (threshold range 480–490) and red (490–500), and the other with a threshold range of 100–250 (100% opacity level), color-rendered in blue.

In correlation with the actual outer-wall configurations of the aneurysmal complex and the perianeurysmal structures observed at microneurosurgery, reconstructed images were compared with the intraoperative visual data recorded on the digital videotapes. The characteristics of the aneurysmal complex—including relationship of an aneurysm to the parent arteries, shape and surface features of the aneurysmal neck and dome, contact and adhesion with the perianeurysmal structures—were evaluated independently by five neurosurgeons (T.S., A.K., Y.Y., S.T., K.O.), including an operator. By using reconstruction parameters of a function curve saved on the workstation, each conventional and transparent 3D MR cisternogram could be reproducible within approximately 20 seconds after MR imaging.

Case 1

An 83-year-old woman presented with an unruptured right internal carotid–posterior communicating artery and a small anterior choroidal artery aneurysm. The operative photograph (Fig 2A) showed the caudal view of the right superolateral aspect of those aneurysms and perianeurysmal structures, including the right optic nerve surrounding the cranial base bone and adjacent brain. The posterior communicating artery aneurysm (9.8 × 8.4 mm) extended laterally, with a large dome showing a slightly convex surface. By dissecting the distal margin of the posterior communicating artery aneurysm, a small anterior choroidal artery aneurysm (2.5 × 1.8 mm) arising from the internal carotid artery was observed. The digital subtraction angiogram (Fig 2B), right oblique projection, showed both a large posterior communicating artery aneurysm and a well-demarcated small anterior choroidal artery aneurysm. The 3D MR angiogram (Fig 2C), obtained using a similar projection as that of the operative view (Fig 2A), showed the arterial components of the aneurysmal complex; findings of the 3D MR angiogram were similar to those of the operative view but differed slightly in surface features of the aneurysmal neck and dome. The minimum intensity projection (MinIP) image of the source axial MR cisternogram (Fig 2D), superoinferior projection, depicted the posterior communicating artery aneurysm, the optic nerve and optic chiasma, the anterior and posterior clinoid process bones, the petroclinoidal dural fold, and the adjacent temporal lobe. The conventional 3D MR cisternogram (Fig 2E), obtained by using a similar projection to that of the operative view, showed the spatial expansion and contact of the aneurysm with the perianeurysmal structures. The shape and surface features of the neck and dome of the aneurysm, and their relationship to the parent arteries and the temporal lobe, were essentially comparable to the operative findings. The distal margin of the posterior communicating artery aneurysm, however, was indistinguishable from the proximal margin of the anterior choroidal artery aneurysm because of the adhesive contact of aneurysmal margins before surgical dissection. The virtual viewpoint of the 3D MR cisternogram (Fig 2F), superoposterior projection, showed an unclear border between the two aneurysms and contact of the internal carotid–posterior communicating artery aneurysm with the temporal lobe.

Case 2

A 54-year-old man presented with an unruptured left internal carotid–posterior communicating artery aneurysm. The operative photographs (Fig 3A and B) showed the caudal view of the left lateral aspect of the aneurysmal complex. The aneurysm (2.5 × 2.7 mm) arose from the internal carotid artery distal to the posterior communicating artery branch and extended laterally. Most of the dome was embedded in the adjacent temporal lobe. By dissecting the margin of the dome from the brain, the whole shape of the aneurysm appeared with a round bleb at the tip. The 3D MR angiogram (Fig 3C), obtained using a similar projection to those of the operative views (Fig 3A and B), showed the aneurysmal complex, which appeared to be similar but slightly different owing to aneurysmal shape and small protrusions on the surface of parent artery at the contralateral side of the neck. The 3D CT angiogram (Fig 3D), obtained by using a similar projection to those of the operative views, showed the aneurysmal complex and cranial base bone similarly. The conventional 3D MR cisternogram (Fig 3E), obtained by using a similar projection to those of the operative views, showed the spatial relationship between the parent internal carotid artery, the aneurysmal neck, the posterior clinoid process bone, the petroclinoidal dural fold, and the temporal lobe. The transparent 3D MR cisternogram (Fig 3F) depicted the aneurysmal complex transparently through the vessel wall and the adjacent brain. Those features correlated well with the operative findings, but the MR cisternographic findings did not precisely match those of the actual operative

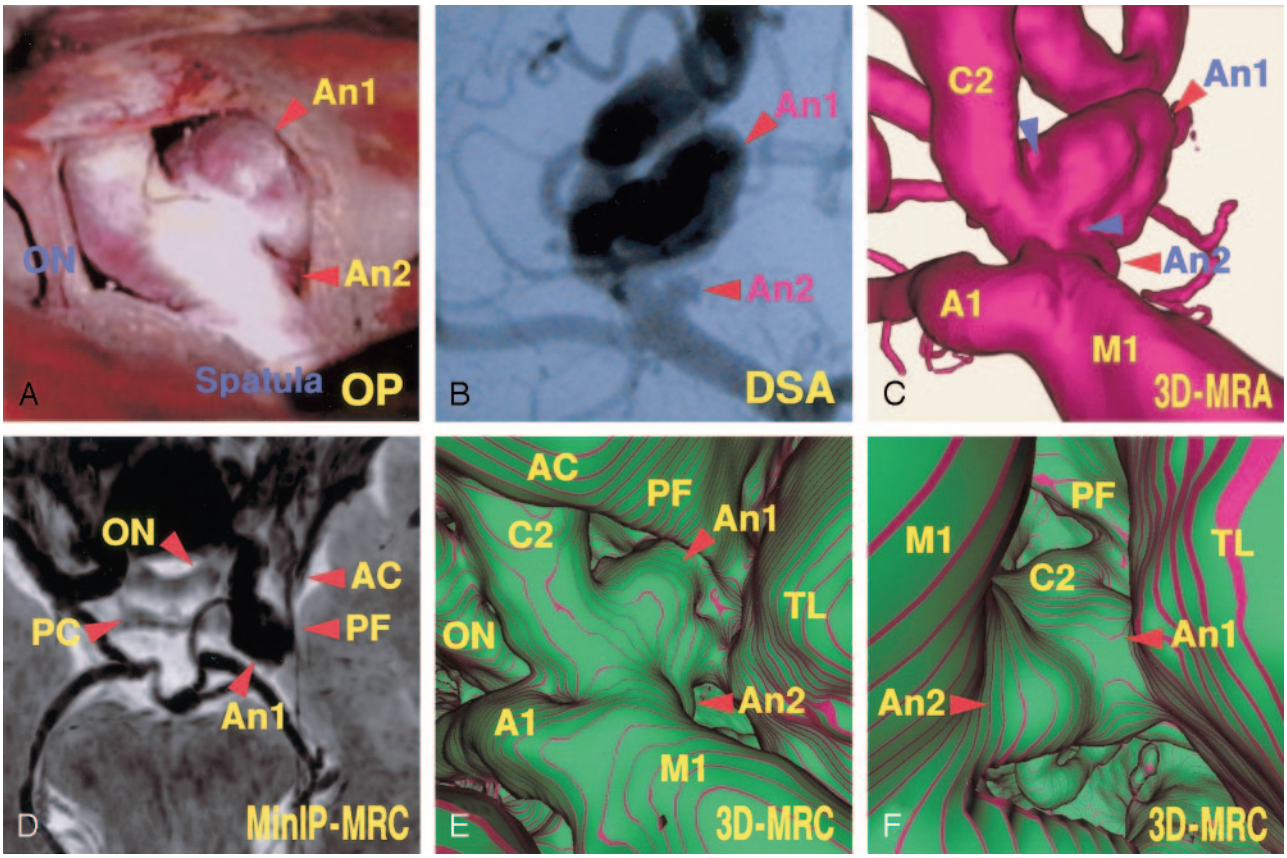

FIG 2. Case 1, an 83-year-old woman with a large unruptured right internal carotid–posterior communicating artery aneurysm and a small anterior choroidal artery aneurysm.

A, Operative photograph showing the caudal view of the right superolateral aspect of the posterior communicating artery aneurysm (An 1), the anterior choroidal artery aneurysm (An 2), and the right optic nerve (ON).

B, Digital subtraction angiogram, right oblique projection, showing the aneurysms (An 1, An 2).

C, 3D MR angiogram, similar projection to the operative view in panel *A,* showing the arterial components of the aneurysmal complex. Note the slightly concave surface at the neck (*arrowheads*).

D, MinIP image obtained from MR cisternography, superoinferior projection, showing the cisternal structures with negative shadows in contrast to the surrounding CSF with a positive shadow. ON, optic nerve; AC, anterior clinoid process; PC, posterior clinoid process; PF, petroclinoid dural fold.

E, Conventional 3D MR cisternogram, similar projection to the operative view in panel *A,* depicting the contours of the aneurysmal complex (An 1, An 2, A1, C2, M1), the right optic nerve (ON), the anterior clinoid process (AC), the petroclinoidal dural fold (PF), and the temporal lobe (TL).

F, Conventional 3D MR cisternogram, virtual viewpoint from superoposterior projection, showing the aneurysmal complex and perianeurysmal environment.

field because of the change in position of the frontal lobe and dissection of the soft tissue by intraoperative manipulation and retraction in surgical extension.

Discussion

Current advances in vascular imaging techniques—including MR angiography (3–6), CT angiography (2, 7), and rotational digital subtraction angiography (8)—provide invaluable information regarding the angioarchitecture of a cerebral aneurysm. The 3D images reconstructed from these angiograms by using computer medical visualization software represent the spatial relationship between parent arteries and an aneurysm. Because these angiograms depict angioarchitecture with fine intraluminal configurations, contours or actual outer wall features of the vessels and an aneurysm observed at microneurosurgery are similar but slightly different in certain cases. A discrepancy often exists between angiographic and the intraoperative findings, especially in cases of aneurysms with intra-aneurysmal thrombus or a thick atherosclerotic wall. In addition, the spatial anatomic relationship of aneurysmal contours to the perianeurysmal structures is not depicted precisely on the conventional angiograms.

In contrast, MR cisternography (9–11) depicts the vascular structures, including vessels and aneurysms, with profoundly low signal intensity; cranial nerves and brain parenchyma with moderately low signal intensity; and cranial base bones with variably low to high signal intensities. Thus, the space-occupying intra- and juxtacisternal structures are well demarcated by the profoundly hyperintense adjacent subarachnoid CSF. These cisternographic features may be useful in depicting the aneurysmal contours with perianeurysmal structures. The ability of MR cisternog-

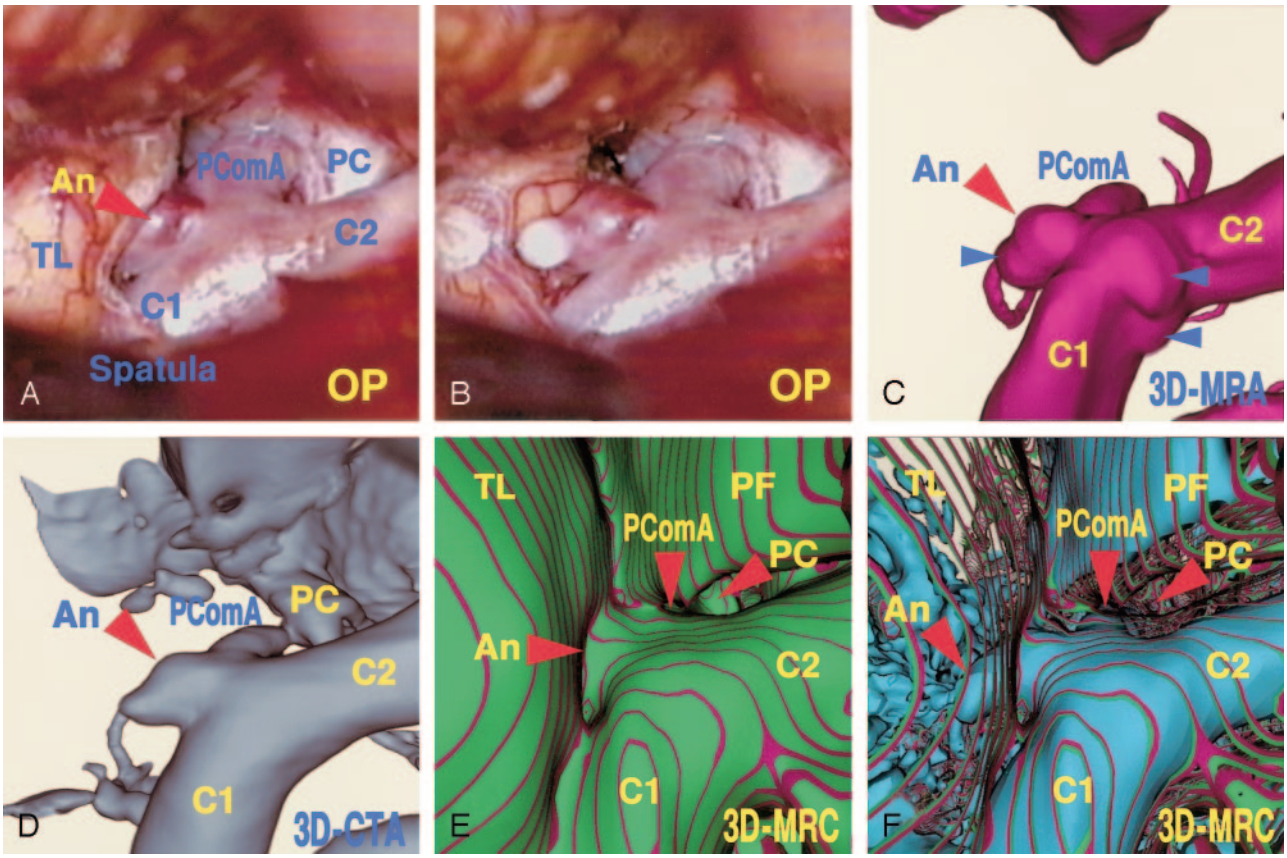

FIG 3. Case 2, a 54-year-old man with an unruptured left internal carotid–posterior communicating artery aneurysm.

Operative photographs before (*A*) and after (*B*) surgical dissection of the embedded aneurysmal dome, showing the aneurysm (An), the internal carotid artery (C1, C2), the posterior communicating artery (PComA), posterior clinoid process (PC), and the temporal lobe (TL).

C, 3D MR angiogram, similar projection to the operative views in panels *A* and *B,* showing the aneurysmal complex. Note the slight difference in terms of the aneurysmal shape and small protrusions on the parent artery (*arrowheads*).

D, 3D CT angiogram, similar projection with the operative views in panels *A* and *B,* showing the aneurysmal complex and cranial base bone similarly.

E, Conventional 3D MR cisternogram, similar projection to the operative views in panels *A* and *B,* depicting the contours of the aneurysmal complex (An, C1, C2, PComA), the posterior clinoid process bone (PC), the petroclinoidal dural fold (PF), and the temporal lobe (TL).

F, Transparent 3D MR cisternogram, the same projection as in panel *E,* depicting the whole shape of the aneurysm (An) and parent arteries (C1, C2, PComA) in blue, transparently through the vessel wall and the adjacent brain surface (green and red).

raphy to reveal spatial relationships of the aneurysmal complex to the perianeurysmal structures may, however, be limited by the 2D assessment based on review of one or more source images.

By using the 3D reconstruction technique with a perspective volume-rendering algorithm (1, 2), information regarding the entire area with lower signal intensity than CSF can be selected from the whole volume-rendering data set without targeting or trimming of the region of interest obtained by the MR cisternography. The conventional 3D MR cisternograms can provide an extensive spatial view of the cisternal structures including the aneurysmal complex and perianeurysmal structures, from various viewpoints within the subarachnoid cisternal space; these images may not be identical, but the shape and surface features of the aneurysmal neck and dome and their relationship to the parent arteries and periaeurysmal environment are correlated well with the operative findings. Because retraction of the brain and dissection of the soft tissue are usually performed during surgical manipulation, the preoperative image is different from the intraoperative field in the detail. The movement of the intra- and juxtacisternal structures following surgical exposure always compromises comparison of those pre- and intraoperative studies. In addition, the transparent 3D MR cisternogram, reconstructed by using a perspective volume-rendering algorithm with transluminal imaging technique (2–4), allows borderline imaging with selected volume data; contours of the foreground objects are depicted as a series of rings, so that the underlying objects visualized directly through the spaces between rings. In a case of an embedded aneurysm, the whole shape of the aneurysm could be depicted transparently through the surrounding brain parenchyma.

Assessment of the anatomic relationship between the aneurysmal complex and the perianeurysmal environment on the preoperative 3D MR cisternograms can provide useful information, not only in the surgi-

cal or interventional managements, but also for investigating the natural history of unruptured cerebral aneurysms. In addition to the intrinsic factors related to the initiation, growth, and rupture of cerebral aneurysms—including the geometric angioarchitecture, morphology of the dome, pathologic fragility of the wall, and intraaneurysmal flow dynamics—outer wall configurations of the aneurysm and the surrounding intra- and juxtacisternal structures may play a role in the development of cranial nerve symptoms or in the deformation of the aneurysmal shape (9, 12); contact of an aneurysm with the perianeurysmal environment may affect the growth and rupture of an unruptured cerebral aneurysm.

Although the 3D MR cisternogram depicts the contours of the intra- and juxtacisternal structures transparently through the intermediating CSF, several limitations may exist in the application of 3D MR cisternography. First, the quality of the 3D MR cisternogram depends on the degree of spatial and signal intensity resolution obtained by the source MR cisternogram (9–11). With the present imaging equipment, the fine structures such as arachnoid trabecula, small veins, and perforating arteries within the cistern may not be depicted, but higher field strength imager and alternative imaging sequences, including 3D constructive interference in the steady state and 3D fast asymmetric spin echo, may provide higher spatial resolution with better signal-to-noise ratios (10, 11). In addition, the pulsation and flow-related artifacts appearing within the subarachnoid CSF space, the vessels, and an aneurysm may affect the MR imaging signal intensity (10).

A second limitation is related to reconstruction of the image by using a volume-rendering algorithm (1–6). A postprocessing computer medical visualization software offers numeric imaging analysis of the 3D reconstructed volume-rendering data set and then depicts the specific results as a computer-generated 3D image. The magnitude of signal intensity of the MR cisternography, however, varies among individuals and imaging sequences, and according to the conditions of examination, the threshold values of signal intensity for CSF and cisternal structures are difficult to define. In cases of the perianeurysmal objects showing similar signal intensity to the surrounding CSF, it may be difficult to distinguish the boundary of the aneurysmal contour. The diameter of the intra- and juxtacisternal structures is variable depending on the MR imaging signal intensity values selected for their contours. So that the signal intensity threshold of the opacity curve should not be fixed to the specific values, but must be optimized on the basis of the signal intensity histogram drawn on each source image of the MR cisternogram. For the reproducible and reliable assessment with the 3D MR cisternogram, further adjustment of threshold range may be necessary to refine the contours in each object in correlation with the actual intraoperative findings.

A third limitation depends on the restricted anatomic cisternal space of CSF. The extent of the aneurysmal complex visualized by 3D MR cisternography is essentially limited within the subarachnoid cisternal space. Visual access for conventional 3D MR cisternography is restricted within the cisternal space through the limited projections and viewing angles but may be useful in considering the surgical approach and simulating surgical exposure. Transparent 3D MR citernography may partially overcome the above-mentioned limitation and provide a transparent view of cisternal structures. Multiprojection assessment with 3D MR cisternography, in conjunction with MR angiography, CT angiography, and digital subtraction angiography is necessary in investigating the aneurysmal angioarchitecture.

Conclusion

By using a perspective volume-rendering algorithm with transluminal imaging technique, reconstruction of the MR cisternogram obtained by a T2-weighted 3D fast spin-echo sequence offers 3D visualization of the contours of the cisternal structures including an aneurysmal complex and intracisternal cranial nerve and juxtacisternal brain; this visualization is comparable to operative findings. Pretreatment clinical assessment of the aneurysmal contours and perianeurysmal environment would be useful in considering therapeutic management of cerebral aneurysms with surgical or interventional procedures. In addition, because the contact of aneurysm with the perianeurysmal environment may cause compression of the adjacent cranial nerve or deformation in aneurysmal shape, 3D MR cisternography can provide useful information for investigating the natural history of an unruptured cerebral aneurysm.

References

1. Rubin GD, Beaulieu CF, Argiro V, et al. **Perspective volume rendering of CT and MR images. Application for endoscopic imaging.** *Radiology* 1996;199:321–330
2. Satoh T. **Transluminal imaging with perspective volume rendering of computed tomographic angiography for the delineation of cerebral aneurysms.** *Neurol Med Chir (Tokyo)* 2001;41:425–430
3. Satoh T, Onoda K, Tsuchimoto S. **Visualization of intraaneurysmal flow patterns with transluminal flow images of 3D MR angiograms in conjunction with aneurysmal configurations.** *AJNR Am J Neuroradiol* 2003;24:1436–1445
4. Satoh T, Onoda K, Tsuchimoto S. **Intraoperative evaluation of aneurysmal architecture: comparative study with transluminal images of 3D MR and CT angiograms.** *AJNR Am J Neuroradiol* 2003;24:1975–1981
5. Maeder PP, Meuli RA, de Tribolet N. **Three-dimensional volume rendering for magnetic resonance angiography in the screening and preoperative workup of intracranial aneurysms.** *J Neurosurg* 1996;85:1050–1055
6. Adams WM, Laitt RD, Jackson A. **The role of MR angiography in the pretreatment assessment of intracranial aneurysms: a comparative study.** *AJNR AM J Neuroradiol* 2000;21:1618–1628
7. Kato Y, Nair S, Sano H, et al. **Multi-slice 3D-CTA: an improvement over single slice helical CTA for cerebral aneurysms.** *Acta Neurochir (Wien)* 2002;144:715–722
8. Tanoue S, Kiyosue H, Kenai H, et al. **Three-dimensional reconstructed images after rotational angiography in the evaluation of intracranial aneurysms: surgical correlation.** *Neurosurgery* 2000;47:866–871

9. Rubinstein D, Sandberg EJ, Breeze RE, et al. **T2-weighted three-dimensional turbo spin-echo MR of intracranial aneurysms.** *AJNR Am J Neuroradiol* 1997;18:1939–1943
10. Mamata Y, Muro I, Matsumae M, et al. **Magnetic resonance cisternography for visualization of intracranial fine structures.** *J Neurosurg* 1998;88:670–678
11. Naganawa S, Koshikawa T, Fukatsu H, et al. **MR cisternography of the cerebellopontine angle: comparison of three-dimensional fast asymmetrical spin-echo and three-dimensional constructive interference in the steady-state sequences.** *AJNR Am J Neuroradiol* 2001;22:1179–1185
12. Ruiz DSM, Tokunaga K, Dehdashti AR, et al. **Is the rupture of cerebral berry aneurysms influenced by the perianeurysmal environment?** *Acta Neurochir Suppl* 2002;82:31–34